Simple and Efficient Visualization of Aromaticity: Bond Currents Calculated from NICS Values

Author(s):
Paenurk, Eno; Gershoni-Poranne, Renana

Publication date:
2022-04-21

Permanent link:
https://doi.org/10.3929/ethz-b-000531278

Originally published in:
Physical Chemistry Chemical Physics 24(15), https://doi.org/10.1039/d1cp05757j

Simple and Efficient Visualization of Aromaticity: Bond Currents Calculated from NICS Values

Eno Paenurk*[,a] and Renana Gershoni-Poranne*[,a,b]

[a] *Laboratorium für Organische Chemie, Department of Chemistry and Applied Biosciences, ETH Zürich, 8093 Zürich, Switzerland*
[b] *Schulich Faculty of Chemistry, Technion – Israel Institute of Technology, Haifa 32000, Israel*

Abstract

Aromaticity is a fundamental concept in chemistry, underpinning the properties and reactivity of many organic compounds and materials. The ability to easily and accurately discern aromatic behavior is key to leveraging it as a design element, yet most aromaticity metrics struggle to combine accurate quantitative evaluation, intuitive interpretability, and user-friendliness. We introduce a new method, NICS2BC, which uses simple and inexpensive NICS calculations to generate information-rich and easily-interpreted bond-current graphs. We test the quantitative and qualitative characterizations afforded by NICS2BC for a selection of molecules of varying structural and electronic complexity to demonstrate its accuracy and ease of analysis. Moreover, we show that NICS2BC successfully identifies ring-current patterns in molecules known to be difficult cases to interpret with NICS, and enables deeper understanding of local aromaticity trends, demonstrating that our method adds additional insight.

Introduction

Aromatic molecules have long captured the imagination of chemists, both for the synthetic challenges they pose and for the opportunities they provide to investigate this elusive property. Recent reports demonstrating this ongoing interest include the preparation of highly anti-aromatic s-indacene derivatives,[1] the discovery of novel carbon allotropes,[2] and the on-surface synthesis of graphene-based structures.[3] In addition, due to the prevalence of polycyclic aromatic molecules as functional materials (e.g., photoswitches,[4] emitters,[5] dyes,[6] organic semiconductors,[7–11] and many others), aromaticity has emerged as a potential design element for tuning important molecular properties, e.g., HOMO-LUMO[12,13] or singlet-triplet energy gap.[14–18] Thus, the ability to identify and quantify aromaticity in such systems is a promising tool for the construction and characterization of novel compounds.

There are myriad approaches and techniques for quantifying aromaticity, stemming from the four main criteria in which it manifests—energetic, geometric, magnetic, and electronic—which are discussed extensively in the book recently edited by Fernandez.[19] Among these, the methods that evaluate the induced ring current and the resulting induced magnetic field share

a particular advantage: they describe physical properties with spatial distributions, which can be mapped onto the molecular structure. As noted by Sundholm et al., the current density itself is a subobservable that can, in principle, be accessed experimentally, though there is to date no experimental procedure to do so. However, it can be calculated as the expectation value of a quantum-mechanical operator.[22] Moreover, computational techniques allow us to specifically distinguish the contribution of the π-electrons to the current density—a separation that would not be feasible experimentally. As it is the π-electron delocalization and its resulting current density that are associated with aromaticity, it is imperative to analyze only these contributions.

Because the human eye is adept at recognizing patterns and features in spatial distributions,[23] such visualizations of chemical properties enable quick and intuitive understanding of molecular behavior,[24–26] in this case, of aromaticity. Though the same information can be conveyed numerically or textually, the clarity and context are significantly enhanced by the visual depiction. Put succinctly, as the adage says, "a picture is worth a thousand words." In Figure 1, we demonstrate the various numerical and visual aromaticity evaluators for anthracene (**CC7**, Scheme 2). We note that, in general, there is a continued interest in visualizing abstract chemical phenomena, as is demonstrated by the recent publications detailing such methods for, e.g., dispersion forces,[27] strain[28] and Clar sextets in polybenzenoid hydrocarbons.[29]

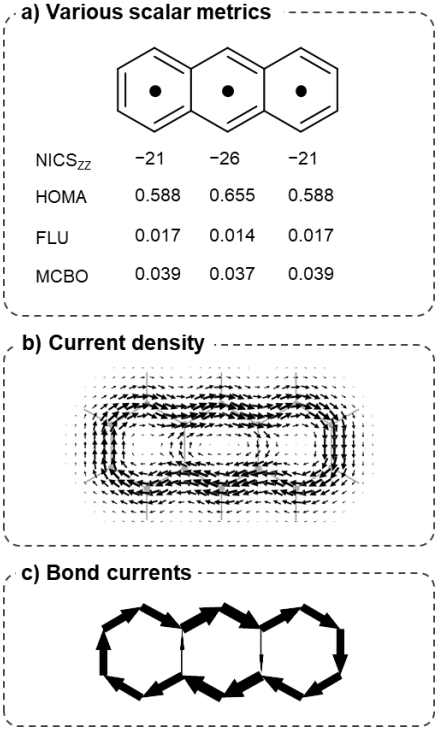

Figure 1. Comparison of various aromaticity evaluations for anthracene (**CC7**). a) Scalar metrics: NICS$_{ZZ}$,[30,31] HOMA,[32,33] FLU,[34] MCBO,[35] calculated with Multiwfn.[36] NICS values are calculated 1 Å above the centers of

the rings (shown by black dots) and reported in ppm units, all other metrics are unitless. b) Current density, calculated with SYSMOIC[37] and visualized with in-house Python code. c) Bond-currents, calculated with SYSMOIC[37] by integration of the current density, visualized with BC-Wizard (see Computational details).

In the study of aromaticity, despite the clear advantages of pictorial depiction, π-electron current density visualization methods are not the most widely used. This is because, for a visualization to be valuable, it should be an accurate and clear representation of the chemical information and, ideally, also easy to generate and analyze. Paradoxically, the same information-richness that makes current density plots intuitive to understand also makes them difficult to use (e.g., to compare different systems, to discern clear patterns of behavior). These difficulties can be somewhat mitigated by using bond-currents, which reduce the complexity by integrating the current density and mapping the result to the molecular structure (e.g., Figure 1c). The calculation of π-electron bond-currents has a long history in the characterization of aromatic molecules[38–40] and has recently enjoyed renewed popularity.[41–51] However, this method has not yet gained widespread use, most likely due to the technical difficulty of obtaining the bond-currents—via integration,[52,53] graph theoretical,[54] or topological[55,56] methods. Similarly to the methods or programs that calculate the current density (e.g., SYSMOIC,[37] GIMIC,[21] ACID[20]), the calculation of bond-currents often also requires more user-expertise and is not as readily accessible to the broader audience of chemists. Hence, despite their advantages, these methods do not manage to combine the requirements of clarity and ease-of-use, and are therefore relatively sparingly used. In most cases, the resulting visual does not allow clear qualitative interpretation, let alone quantitative assessment.

Rather, the most commonly used aromaticity method is the Nucleus Independent Chemical Shift (NICS) method, [30,31,57,58] the basic concept of which is similar to NMR. From a practical perspective, NICS is very easy to use, allows straightforward comparison between systems, and can be calculated with all popular quantum chemical computational software. However, one must recognize that NICS is a proxy for the actual physical property that is the manifestation of aromaticity (i.e., the ring current).[59–63] This also has practical consequences: NICS values are obtained by integrating over the entire current density vector field, which results in loss of spatial information. Thus, it is not uncommon that NICS results are misinterpreted and local/global currents are mischaracterized.[31,64,65] While more informative NICS-based methods exist, such as the NICS-XY-Scan[66] or NICS isosurfaces,[67] the interpretation of NICS in terms of current densities is not intuitive and can lead to mistakes in identification of local and global current pathways.[68]

Herein, we propose a new method, NICS2BC, for generating quantitative bond-current graphs from NICS values. Our approach capitalizes on the individual strengths of the two techniques: it uses simple and inexpensive NICS calculations to afford an intuitively and easily interpretable visual depiction of π-electron bond-currents. We demonstrate here the generality of our method by applying it to representative molecules and comparing our results to those obtained with other techniques. In all cases, the NICS2BC map distills the salient features of the current flow and portrays them in a clear and unambiguous manner. In addition to its visual appeal, we show that NICS2BC successfully deals with cases where interpretations based only on NICS are difficult or ambiguous. Furthermore, the formulation of our method defines a "weight" term for each ring, which essentially translates into a local aromaticity evaluator. To our knowledge, this is the first time NICS values of polycyclic molecules have been deconvolved in such a manner. To clarify, throughout this text, we use the term "aromaticity" to refer specifically to "magnetic aromaticity", i.e., the characterization based on the ring-current model.[59–63]

Computational details

The geometries of all molecules were optimized with Gaussian 09 Revision D.01[69] using the B3LYP[70–73]/def2-TZVP[74] combination with the D3 dispersion correction.[75] All optimized geometries are provided in the SI. For all molecules, NICS calculations were performed with Gaussian using the B3LYP/6-311G(d,p) combination and the gauge-including atomic orbital (GIAO) method for NICS probes at heights of 0.00, 0.25, 0.50, 0.75, 1.00, 1.25, 1.50, 1.50, 1.75, and 2.00 Å above the centers of the rings. From the NICS calculations, $NICS_{ZZ}$ values were extracted for all molecules and all heights. For the CC set of molecules (Scheme 2), we also performed natural chemical shielding (NCS)[76] calculations using the NBO 6[77,78] software interfacing with Gaussian, to dissect the σ and π contributions to the NICS values and obtain $NICS_{\pi ZZ}$ values. The π-orbitals were automatically identified by SYSMOIC[37] and verified by visual inspection.

For all molecules, wavefunction files were generated with Gaussian using the B3LYP/6-311G(d,p) combination and the continuous set of gauge transformations (CSGT) method.[79] The wavefunction file (.wfx) was used with the SYSMOIC[37] program package to calculate current-density vector fields and integrated bond-currents. Herein we present the results obtained by considering only the π-electrons (i.e., the current density and integrated bond-currents from π-electrons only). For results obtained using total integrated bond-currents (i.e.,

σ + π electrons), see Section S6 in the SI. We note that the integrated bond-currents from π-electrons had a slightly better agreement with the $NICS_{ZZ}$-based bond-currents than with the $NICS_{\pi ZZ}$-based bond-currents. The closer agreement of $NICS_{ZZ}$ with π-currents was also recently reported by Radenković and Đorđević,[49] and this strengthened our decision to use the simpler metric. All current-density plots were visualized with an in-house Python code (available in Section S4.2 in the SI). The integrated bond-currents were visualized with BC-Wizard (available on GitLab: gitlab.com/porannegroup/bcwizard).

NICS2BC bond-currents were calculated according to the algorithm described in the NICS2BC Method section of this report (and the additional details in the accompanying SI). For calculating the $\tilde{\boldsymbol{\sigma}}$ matrix, we set the I_{ref} value to 11.5 nA T^{-1} (cf. Equation S1); this value was found by averaging the total and π-current strengths of benzene (Table S7), and rounding it for simplicity. The procedure was automated and implemented as a module within the BC-Wizard Python program package developed by us, which is freely available online (gitlab.com/porannegroup/bcwizard). In addition to the NICS2BC module, BC-Wizard also includes modules for performing BC2NICS calculations (according to Equation S1 in the SI; for the introductory information of such calculations, see Reference 57), input file preparation, and visualization of integrated bond-currents.

The input templates for all the calculations are provided in Section S4 in the SI.

The NICS2BC Method

As mentioned above, NICS is the most popular method for evaluation of aromaticity, due to its simplicity and accessibility, but these advantages come at the price of reduction in information content.[31] This then begs the question: can NICS values be reverted to recreate the underlying current density? Bultinck and coworkers convincingly showed that one cannot uniquely reconstruct the current density from a set of NICS values.[81] The main reason is that the number of NICS values is usually much smaller than the number of grid points required for a 3D current-density map, and therefore the problem is underdetermined. This implies that reverting NICS to current density is, in principle, achievable but, in practice, unfeasible. Recreating current-flow information from NICS requires one to solve the issue of the undetermined equations.

Bond-currents provide a potential solution to this issue, as they require much fewer grid points than a 3D current-density map. Moreover, we recently observed a very good agreement between $NICS_{ZZ}$ values calculated with density functional theory (DFT) and $NICS_{ZZ}$ values

calculated from bond-currents using the Biot-Savart equation.[80] Based on the surprisingly accurate predictions obtained with this approach, we hypothesized that a scheme converting NICS to unique bond-current graphs could be established.

To summarize the procedure: the bond-currents for each individual ring must follow the continuity equation, which leads to each ring effectively having a uniform ring current, consisting of the bond-currents, of some specific strength. We express this current strength with relation to a reference strength (I_{ref}, usually set to be the bond-current strength of the C-C bonds in benzene), such that each ring only carries information about the relation to I_{ref}, which is denoted as the weight of that ring. As a result, the total bond-current graph is now fully determined by the weights of the monocyclic subunits, which sufficiently reduces the dimensionality of the problem to render it solvable. In other words, within this framework of our assumptions and definitions, the number of variables that need to be determined equals the number of rings in the system and, therefore, the problem can be solved with one NICS value per monocyclic subunit. The full derivation is detailed below.

Throughout our derivation, we refer to polycyclic systems and the monocyclic subunits contained within them as directed graphs. Therefore, we first define these graphs, using the example of naphthalene. Scheme 1a shows the full directed graph of naphthalene (**CC4**), where each bond is denoted as a vector between the two respective atoms. Scheme 1b shows the directed graphs of the two individual monocyclic subunits in naphthalene. The directions of the vectors in the full directed graph are, in principle, arbitrary; they only determine the sign of the bond-current strengths used to generate the final bond-current graphs (Scheme 1c).

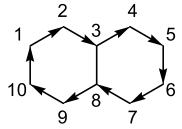

(a) Full directed graph

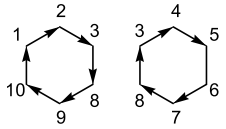

(b) Monocyclic subunit directed graph

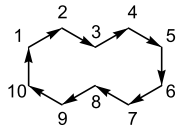

(c) Final bond-current graph

Scheme 1. Graph examples for naphthalene. The numbers indicate the atom indices and the direction of the arrow indicates the direction of the bond vector.

Let us consider the Biot-Savart equation for calculating the induced magnetic field $\boldsymbol{B}^{\mathrm{ind}}$ at position $\boldsymbol{r}$ from a line current with strength I along path C:[82]

$$\boldsymbol{B}^{\mathrm{ind}}(\boldsymbol{r}) = \frac{\mu_0}{4\pi} I \int_C \frac{d\boldsymbol{l} \times (\boldsymbol{r} - \boldsymbol{r}')}{|\boldsymbol{r} - \boldsymbol{r}'|^3} \tag{1}$$

where $d\boldsymbol{l}$ is the differential vector at position $\boldsymbol{r}'$ pointing in the direction of the current flow, and μ_0 is the vacuum permeability. For a molecule with N bonds, with each bond i having a bond-current strength I_i, the induced magnetic field at position $\boldsymbol{r}$ can be calculated as the sum of the individual line integrals over all the bonds:

$$\boldsymbol{B}^{\mathrm{ind}}(\boldsymbol{r}) = \frac{\mu_0}{4\pi} \sum_{i=1}^{N} I_i \int_C \frac{d\boldsymbol{l} \times (\boldsymbol{r} - \boldsymbol{r}')}{|\boldsymbol{r} - \boldsymbol{r}'|^3} \tag{2}$$

Next, we state the following assumptions, within which the NICS2BC scheme was developed:

1) Bond-current graphs obey the continuity equation, i.e., the total current is conserved.
2) Bond-current graphs of polycyclic molecules can be constructed as a sum of the constituent monocyclic bond-current graphs, which individually also follow the continuity equation.

The first assumption is an incontrovertible physical principle, although it is not always fulfilled exactly by bond-currents obtained by integration of current densities, as also discussed in the

construction of other bond-current methods.[55] Its numerical consequence is that for a monocyclic molecule, every bond has the same current strength I_{bond}, which we can denote as the ring-current strength:

$$I_{\mathrm{bond}} = I_{\mathrm{ring}} \; \forall \; bond \; \in \; ring \tag{3}$$

The second assumption stems from the fact that any linear combination of bond-currents that obey the continuity equation will naturally produce new bond-currents that also obey the continuity equation. Our scheme defines each bond-current in the total system as a linear combination of the bond-currents in the individual monocyclic subunits; this choice corresponds to using the smallest set of smallest rings definition,[83] and is distinct from other approaches, which consider all possible circuits.[54,55] In accordance with Equation 3, the bond-current strength I_{bond} in a polycyclic molecule is:

$$I_{\mathrm{bond}} = \sum_{\mathrm{ring} \ni \mathrm{bond}} I_{\mathrm{ring}} \tag{4}$$

In this notation, the ring-current strength I_{ring} also carries a sign that depends on the direction of the current flow—i.e., monocyclic ring-current strengths are added with a positive (negative) sign if the respective bond in the monocyclic directed graph is defined in the same (opposite) direction as the bond in the full directed graph. For example, in the left monocyclic directed graph in Scheme 1b, the bond between atoms 3 and 8 is defined in the same direction as in the full directed graph in Scheme 1a (3 → 8), and the value of I_{ring} would thus be added as a positive value; the same bond in the right monocyclic directed graph is in the opposite direction (8 → 3), and would therefore be added as the negative of the respective I_{ring} value. Because the monocyclic ring currents obey the rule of current conservation, it follows that such linearly combined polycyclic bond-current graphs also obey current conservation and thus satisfy the first assumption.

Using the definition in Equation 4, we can now rewrite Equation 2 as:

$$\boldsymbol{B}^{\mathrm{ind}}(\boldsymbol{r}) = \frac{\mu_0}{4\pi} \sum_{i=1}^{N} \left(\sum_{\mathrm{ring} \ni i} I_{\mathrm{ring}} \right) \int_C \frac{d\boldsymbol{l} \times (\boldsymbol{r} - \boldsymbol{r}')}{|\boldsymbol{r} - \boldsymbol{r}'|^3} \tag{5}$$

Due to the linearity property of integration (the integral of a sum equals the sum of the integrals), we can rearrange this equation to sum over all the rings j in a polycyclic molecule

of M monocyclic subunits (rings), where for each ring we sum over bonds i that belong to that ring:

$$\boldsymbol{B}^{\mathrm{ind}}(\boldsymbol{r}) = \frac{\mu_0}{4\pi}\sum_{j=1}^{M} I_j \sum_{i \in j} \int_{C_i} \frac{d\boldsymbol{l} \times (\boldsymbol{r} - \boldsymbol{r}')}{|\boldsymbol{r} - \boldsymbol{r}'|^3} \tag{6}$$

To simplify the notation, we first define the ring-current strength I_j of ring j as a product of a reference ring-current strength I_{ref} and the weight of the ring w_j. This definition shifts the variable from being a ring-current strength to being a weight.

$$\boldsymbol{B}^{\mathrm{ind}}(\boldsymbol{r}) = \frac{\mu_0}{4\pi}\sum_{j=1}^{M} w_j I_{\mathrm{ref}} \sum_{i \in j} \int_{C_i} \frac{d\boldsymbol{l} \times (\boldsymbol{r} - \boldsymbol{r}')}{|\boldsymbol{r} - \boldsymbol{r}'|^3} \tag{7}$$

Now, we can define the unweighted contribution to $\boldsymbol{B}^{\mathrm{ind}}$ from a monocyclic subunit j, parametric with respect to I_{ref}, as $\widetilde{\boldsymbol{B}}_j^{\mathrm{ind}}$:

$$\widetilde{\boldsymbol{B}}_j^{\mathrm{ind}}(\boldsymbol{r}; I_{\mathrm{ref}}) \stackrel{\mathrm{def}}{=} \frac{\mu_0}{4\pi} I_{\mathrm{ref}} \sum_{i \in j} \int_{C_i} \frac{d\boldsymbol{l} \times (\boldsymbol{r} - \boldsymbol{r}')}{|\boldsymbol{r} - \boldsymbol{r}'|^3} \tag{8}$$

For brevity, we drop the parametric notation and rewrite Equation 7 as:

$$\boldsymbol{B}^{\mathrm{ind}}(\boldsymbol{r}) = \sum_{j=1}^{M} w_j \widetilde{\boldsymbol{B}}_j^{\mathrm{ind}}(\boldsymbol{r}) \tag{9}$$

This equation can be easily transformed to apply to NICS calculations. Firstly, we note that in a uniform external magnetic field $\boldsymbol{B}^{\mathrm{ext}}$, the induced magnetic field can be expressed in terms of the chemical shielding tensor $\boldsymbol{\sigma}$ as: $\boldsymbol{B}^{\mathrm{ind}}(r) = -\boldsymbol{\sigma}(\boldsymbol{r})\boldsymbol{B}^{\mathrm{ext}}$.[81] Depending on the specific NICS metric, NICS is defined as the negative of some component of the chemical shielding tensor. In this work, we focus on the scalar $\mathrm{NICS}_{\mathrm{ZZ}}$ metric, which is defined as: $\mathrm{NICS}_{\mathrm{ZZ}} = -\sigma_{\mathrm{ZZ}} = B_{\mathrm{Z}}^{\mathrm{ind}}/B_{\mathrm{Z}}^{\mathrm{ext}}$, where the subscripts denote the component of the tensor or the vector. For notational simplicity and due to the direct connection to the chemical shielding tensor, we denote the scalar NICS value as σ. As the external magnetic field is constant, the $\boldsymbol{B}^{\mathrm{ind}}$ vector in Equation 9 can be trivially substituted by a scalar NICS value:

$$\sigma(\boldsymbol{r}) = \sum_{j=1}^{M} w_j \, \tilde{\sigma}_j(\boldsymbol{r}) \tag{10}$$

When NICS values are calculated at several positions r_i, we have several instances of Equation 10, each corresponding to an expression for the NICS values at the respective position (denoted as $\sigma(\boldsymbol{r}_i) = \sigma_i$. For N NICS values and M monocyclic subunits, we can cast these into the following matrix equation:

$$\begin{pmatrix} \sigma_1 \\ \sigma_2 \\ \vdots \\ \sigma_N \end{pmatrix} = \begin{pmatrix} \tilde{\sigma}_{11} & \tilde{\sigma}_{12} & \cdots & \tilde{\sigma}_{1M} \\ \tilde{\sigma}_{21} & \tilde{\sigma}_{22} & \cdots & \tilde{\sigma}_{2M} \\ \vdots & \vdots & \ddots & \vdots \\ \tilde{\sigma}_{N1} & \tilde{\sigma}_{N2} & \cdots & \tilde{\sigma}_{NM} \end{pmatrix} \begin{pmatrix} w_1 \\ w_2 \\ \vdots \\ w_M \end{pmatrix} \tag{21}$$

where $\tilde{\sigma}_{ij}$ denotes the contribution of the *j*-th ring to the *i*-th σ value, w_j is the weight of the *j*-th ring, and σ_i is the *i*-th NICS value (Figure 2b). We can write this equation in condensed notation as:

$$\vec{\sigma} = \tilde{\boldsymbol{\sigma}}\vec{w} \tag{12}$$

To solve for the weights, we need to invert this equation. If the number of rings (*M*) is equal to the number of NICS probes (*N*) and the matrix $\tilde{\boldsymbol{\sigma}}$ is invertible, then the weights can be calculated by multiplying Equation 2 from the left by the inverse of $\tilde{\boldsymbol{\sigma}}$ (Equation 13). If N > M, we can multiply from the left by the pseuso-inverse of $\tilde{\boldsymbol{\sigma}}$ (Equation 14).

$$\vec{w} = \tilde{\boldsymbol{\sigma}}^{-1}\vec{\sigma} \tag{13}$$

$$\vec{w} = (\tilde{\boldsymbol{\sigma}}^{\mathrm{T}}\tilde{\boldsymbol{\sigma}})^{-1}\tilde{\boldsymbol{\sigma}}^{\mathrm{T}}\vec{\sigma} \tag{14}$$

In these equations, $\vec{\sigma}$ vector contains the input NICS values which are converted to the weights and the $\tilde{\boldsymbol{\sigma}}$ matrix can be populated by various means, e.g., with the Biot-Savart equation (cf. Equation S1 in the SI) or with a Hückel-like parametrized approach (Section S2 in the SI). All of the results presented in this text were obtained with the Biot-Savart equation.

Once the weights have been calculated, the third step is to construct the bond-current graphs by simply adding the superimposed weighted bond-currents of the monocyclic subunits (Equation 15, Figure 2c).

$$I_{\mathrm{bond}} = \sum_{\mathrm{ring} \ni \mathrm{bond}} w_{\mathrm{ring}} I_{\mathrm{ref}} \tag{15}$$

These I_{bond} values, together with the bond vector definitions (which can be in arbitrary directions as they only matter for the sign of I_{bond}), can then be used to construct bond-current graphs. At the conclusion of the procedure, both the weights of the individual rings and the

molecular bond-currents have been obtained. In other words, information pertaining to both the local and global magnetic behavior of the molecule is afforded.

An illustration of the overall workflow of the NICS2BC method for the example of anthracene (**CC7**, Scheme 2), together with a condensed notation of the relevant equations, is depicted in Figure 2. In this section, we describe the general workflow of NICS2BC; for details on how to run the BC-Wizard program that automates the NICS2BC procedure, we refer the reader to the documentation.

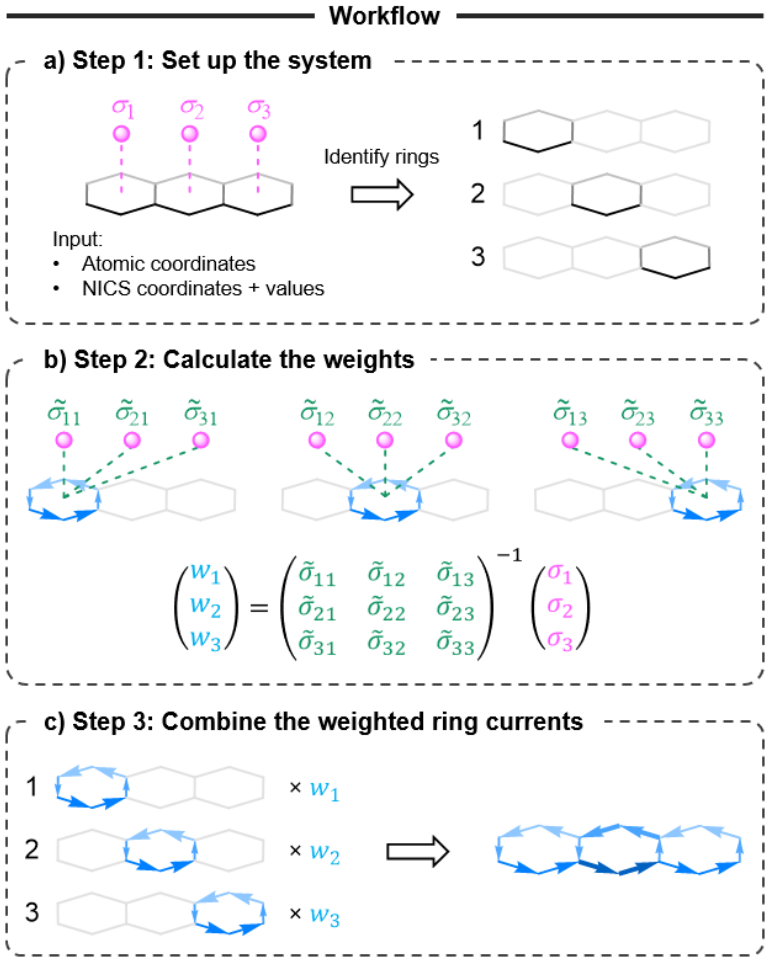

Figure 2. The general workflow of the NICS2BC scheme exemplified on anthracene (**CC7**).

It is worth emphasizing that, to the best of our knowledge, NICS2BC is the first method that enables calculation of the π-electron contribution to the current strength using the GIAO (gauge-including atomic orbitals)[79,84] framework. To date, this has only been achieved within the ipsocentric approach.[85]

Results and Discussion

To ensure that our bond-current visualization method provides trustworthy information, it is necessary to verify that they capture the same behavior, both qualitatively and quantitatively. In other words, we need to ascertain that the bond-currents generated by our method are in the correct directions and magnitudes.

To test this, we created two sets of molecules: a) the *cata*-condensed (CC) set and b) *peri*-condensed (PC) set. The reasoning for this was that each set provided a different test of the method's capabilities. The CC set allowed us to perform a quantitative assessment of our method, because we could compare the predicted bond-currents to those obtained by integration with an independent method (SYSMOIC,[37] developed by Zanasi and coworkers). This quantitative comparison was not possible for the PC set, because the integration of the currents in these molecules by SYSMOIC tended to disobey the continuity equation (see Section S3.1 in the SI). On the other hand, the PC set was much more suited for testing the advantages of our method for qualitative interpretation (i.e., identifying different currents within a polycyclic system). While the CC set was mostly straightforward to interpret, the PC set was more challenging, due to bifurcation of currents and the co-existence of multiple π-circuits. The combination of both of these sets tests the accuracy and generality of NICS2BC for visualizing bond-currents and for interpretation of magnetic behavior in polycyclic systems.

The CC set included 39 mono- and polycyclic systems comprising rings of different size, charge, and aromatic character (depicted in Scheme 2; all molecules except **CC1**− **CC4** and **CC13**−**CC15** were also calculated with +2 charge, see Section S5.1 in the SI for further details).

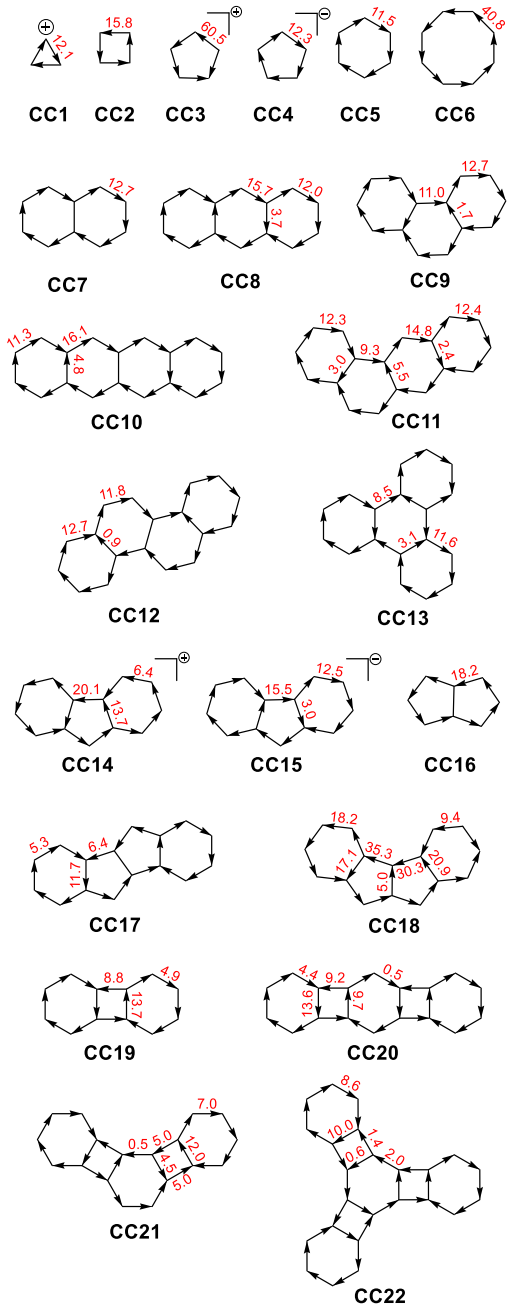

Scheme 2. The cata-condensed (CC) set of molecules used for quantitative assessment of the method. All molecules except **CC1**− **CC4** and **CC13**−**CC15** were also calculated with a charge of +2. The bond-current strength calculated with NICS2BC using the $NICS_{ZZ}$ values are shown in red (only unique values are shown). For the complete set of bond-current values and for the bond-current values of the dicationic systems, see SI.

For each of these molecules, we calculated the bond-currents with our method, using $NICS_{ZZ}$ values extracted from probes placed at 0, 0.25, 0.5, 0.75, 1, 1.25, 1.5, 1.75, and 2.0 Å above the center of each respective ring in the molecule ($NICS_{\pi ZZ}$ values were also calculated at the same heights; for further details see Section S5.2 in the SI). We then compared the bond-currents obtained with our method to bond-currents obtained by integration of the current density field generated by the π-electrons only, calculated using SYSMOIC.[37] As can be seen

in Figure 3, there is an excellent agreement between the bond-currents obtained with the two methods when the NICS probe is placed at a height of 1.25 Å above the ring, agreeing with the recent report by Radenković and Đorđević regarding both the optimal height and the correlation between $NICS_{ZZ}$ and the π-current (see Section S5.2 in the SI for correlations obtained at other heights).[49] This indicates that our approach does indeed reproduce the current susceptibilities of the system, both in size and direction. It is important to note that, in principle, the $NICS_{\pi ZZ}$ metric is considered to be the most accurate NICS-based metric for aromaticity evaluation.[31,86,87] However, it requires more specialized and more expensive calculations. We elected to report here on results obtained using $NICS_{ZZ}$ values in order to demonstrate the generality of the method and the quality of the results, when using the more accessible and computationally inexpensive metric. The quality of the results indicates that the gain in ease-of-use does not come at the cost of accuracy, which is supported a recent report by Berger et al, which also demonstrates the relationship between the $NICS_{ZZ}$ metric and the strength of the ring-current in monocyclic systems.[53] The results obtained with $NICS_{\pi ZZ}$ values are reported in the SI and show very close agreement.

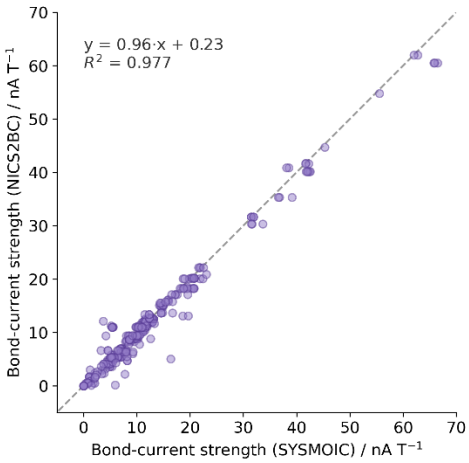

Figure 3. Correlation between bond-current strengths calculated by SYSMOIC (x-axis) and NICS2BC (y-axis), RMSD = 1.8 nA T^{-1}.

To demonstrate the visual nature of NICS2BC and the easy interpretation it enables, Figure 4 shows a comparison between NICS2BC maps and current density maps for representative examples of the CC set (the results for the complete set are provided in Section S5.3 in the SI). Note that diatropic (paratropic) currents, which generally denote aromaticity (antiaromaticity), are shown flowing in the clockwise (counter-clockwise) direction. The analysis of these molecules' aromatic behavior has been previously described in the literature,[66,88] thus we mainly comment on the agreement between the NICS2BC and current-density maps and

describe the main features of the current. In general, the NICS2BC maps replicate the current-density features well. Phenanthrene (CC9, Figure 4a) is largely characterized by a global diatropic current at the periphery, with slightly stronger currents in the side rings. CC18 (below Figure 4b) is characterized by multiple currents, creating an asymmetric current flow whereby the strongest paratropic current is seen in the right-hand 5-membered ring. Biphenylene (CC19, Figure 4c) has diatropic currents in the 6-membered rings and a stronger paratropic current in the 4-membered ring.

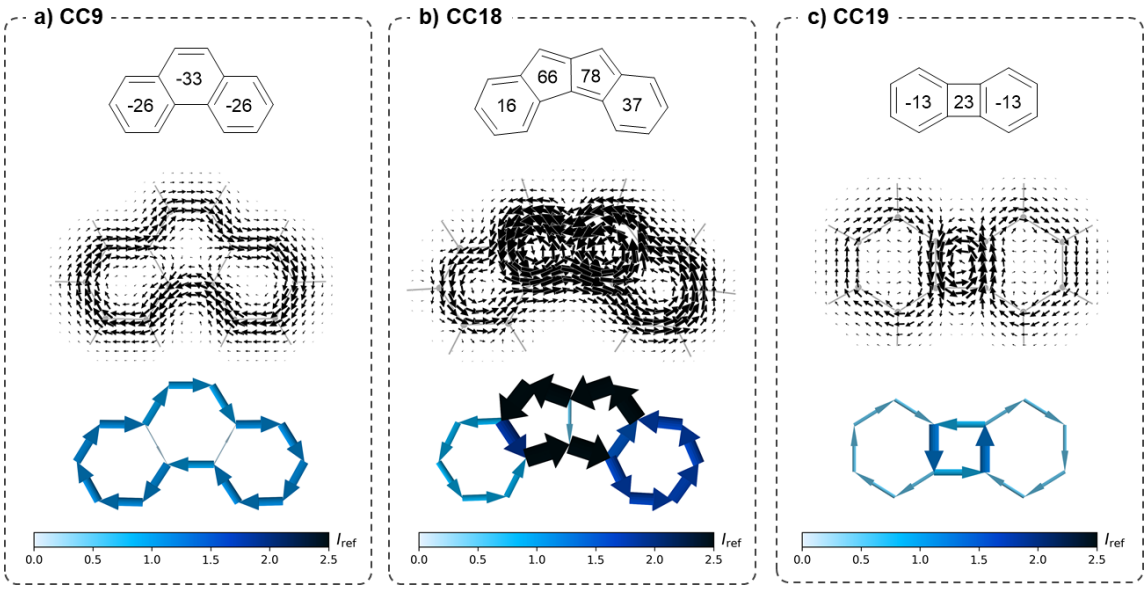

Figure 4. Comparison of NICS2BC and current density maps for representative examples of *cata*-condensed molecules. Top: Scheme of molecule and NICS values above each ring center; Middle: Current-density maps; Bottom: NICS2BC graph for a) **CC9** (phenanthrene); b) **CC18**; c) **CC19** (biphenylene). Current density calculated with SYSMOIC and plotted with in-house Python code at a height of 1.25 Å above the molecular plane. NICS2BC currents calculated from $NICS(1.25)_{ZZ}$, strength is reported relative to I_{ref} (the ring current of benzene, 11.5 nA T^{-1}).

Having established that the description provided by our method is a satisfactory reproduction of the current density for these relatively simple molecules, and having found the optimal height for placing the NICS probe, we then turned to testing the capabilities of NICS2BC in more challenging molecules, i.e., the PC set (Figure 5).

Peri-condensed molecules, in which a single atom is shared by three rings, generally exhibit more complex aromatic behavior than *cata*-condensed molecules, owing to the larger number of individual (and possibly overlapping) π-circuits.[89] We show here a few classic examples of such cases.[89] Certain types of current patterns can arise that might be mischaracterized if NICS values alone are used for interpretation.[90,91] We show here a few classic examples of such cases. The first example is perylene (**PC1**), in which the central ring displays a positive NICS value ($NICS(1.25)_{ZZ}$ = 7 ppm, Figure 5a), which indicates a weak paratropic current. However,

current density maps show that there is no ring current at all flowing in this ring. Instead, the value is a result of the effects of the neighboring rings, where two semi-global diatropic current flow in the disjoint naphthalene units. Though the NICS value itself would suggest a paratropic current, NICS2BC accurately reproduces the true current flow and reveals the lack of current in this ring.

The second example is the case of bifurcating currents,[92] as exemplified in pyrene (**PC2**) and anthanthrene (**PC3**), which is specifically known to be a "hard case" for NICS.[90] In both of these molecules there are rings that have markedly negative NICS values, indicating diatropic currents (for **PC2**: $NICS(1.25)_{ZZ} = -19$ ppm, Figure 5b; for **PC3**: $NICS(1.25)_{ZZ} = -12$ ppm, Figure 5c). Bond-current maps show, however, that these rings have currents flowing in opposite directions branching from the bifurcation point, and thus do not form diatropic ring currents. In these cases, assignment of the aromatic character based solely on the NICS value is, in the best case, ambiguous and, in the worst case, misleading. It is therefore even more remarkable that, using only these same NICS values as input, NICS2BC identifies the bifurcation and replicates the current flow successfully (Figure 5b and 5c).

Another classic example of ambiguity in aromaticity characterization of *peri*-condensed molecules is found in coronene (**PC4**, Figure 5d). All of the rings in coronene have negative NICS values, a result which is consistent with two different interpretations. It was first rationalized that coronene is an "annulene-within-an-annulene",[93,94] whereby there are two diatropic currents, a peripheral and a central one. Subsequently, it was shown that there is actually a central paratropic current and a peripheral diatropic current,[21,95] The interpretation of these counter-rotating currents in terms of aromatic behavior has been debated in the literature, and different approaches have been employed to identify whether the central ring is aromatic or antiaromatic.[96,97] Though the NICS values themselves do not enable unambiguous interpretation, NICS2BC not only successfully replicates the two counter-rotating currents in coronene (Figure 5d), but also enables interpretation of the local aromatic behavior. The weight for each ring (inner ring = 1.23, outer rings = 1.54; see Table S87) provides the magnitude of the ring current with respect to benzene. The positive sign of the weight for the inner ring indicates that it is aromatic, in agreement with the characterization made by others.[96,97]

As an additional test of the method, we applied it to **PC5**, which contains both an 8-membered ring and three types of heterocycles (pyrrole, furan, and thiophene). The NICS2BC map obtained shows that the current flow is well-reproduced, indicating that the presence of

heteroatoms does not adversely affect the ability of the method (Figure 5e). Altogether, these cases demonstrate that NICS2BC can accurately reproduce the current flow in *peri*-condensed molecules of varying structure and aromatic character. In particular, it succeeds in cases for which NICS-based characterization has previously failed.

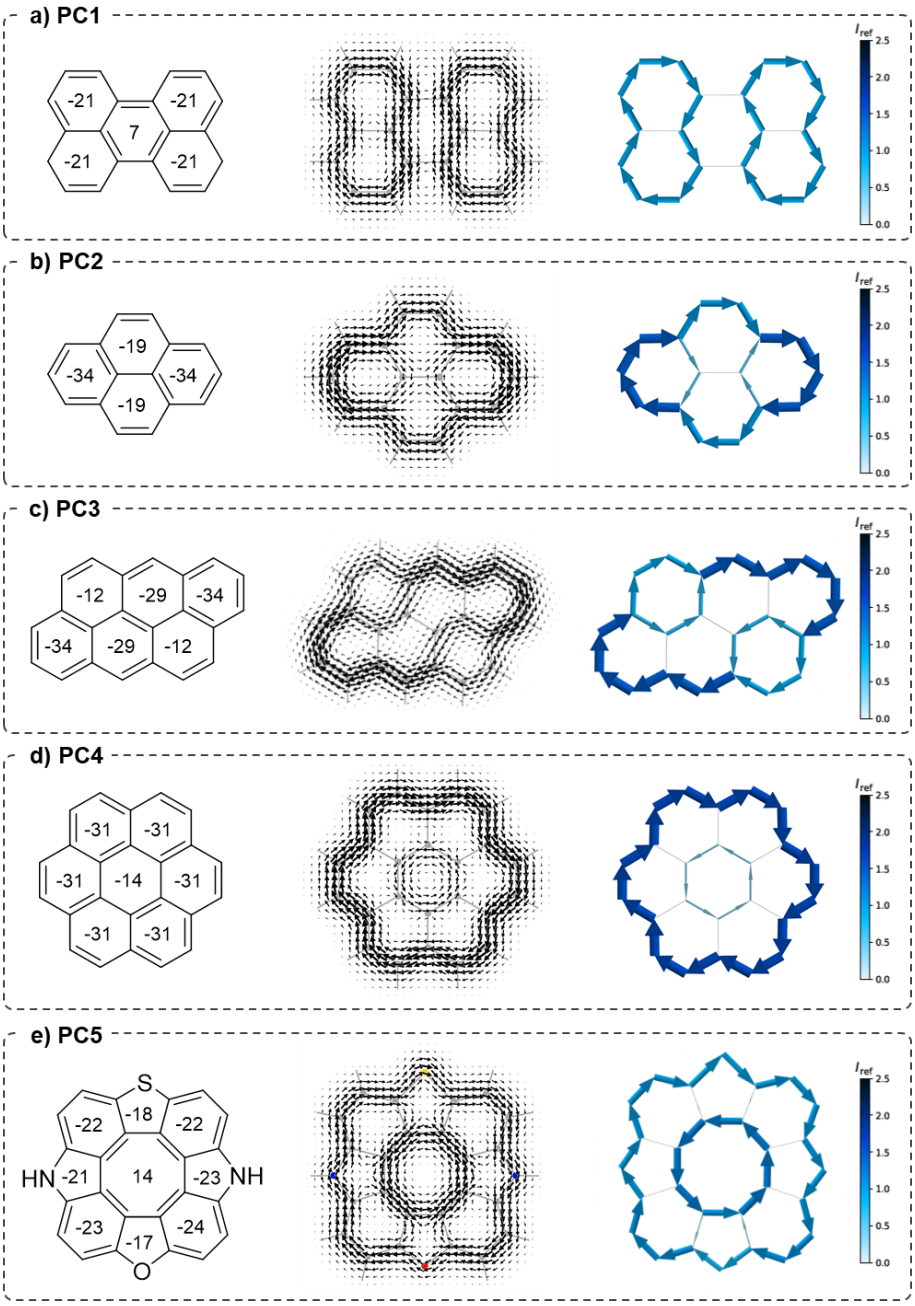

Figure 5. Comparison of NICS2BC and current density maps for representative examples of *peri*-condensed molecules. Left: Scheme of molecule and NICS values above each ring center; Middle: Current-density maps; Right: NICS2BC graphs for a) **PC1** (pyrene); b) **PC2** (perylene); c) **PC3** (anthanthrene); d) **PC4** (coronene); e) **PC5**. Current density calculated with SYSMOIC and plotted with in-house Python code at a height of 1.25 Å above the molecular plane. NICS2BC current calculated from $NICS(1.25)_{ZZ,}$ strength is reported relative to I_{ref} (the ring current of benzene, 11.5 nA T^{-1}).

In all CC and PC cases (Figure 4, Figure 5, and Figures S9-S14 in the SI), the mapping of the arrows to the bonds avoids the ambiguity that can arise from current density maps, for example, at which height one should visualize the current density, and how one should consider arrows going in various directions in the vicinity of a bond. Additionally, the width and color of the arrows showcase the relative strength of the current along different bonds within the molecule, making it simpler to identify regions with weaker/stronger currents at a glance. Remarkably, NICS2BC not only replicates the important features of the current density well and provides a clear picture for interpretation, but it does so by using minimal input (one NICS value per ring).

Finally, we selected two molecules from recent reports in the literature as challenging test cases to assess the capabilities of NICS2BC. **Test1** (triplet-state pentacene, Figure 6a) was computationally characterized by Solà and coworkers[98] and provided an opportunity to test the application of NICS2BC to an open-shell system. **Test2** (Figure 6b) was recently prepared and characterized experimentally and computationally by Müllen and coworkers.[3] This polycyclic system, which contains 23 rings ranging in size from 5- to 7-membered rings, provided an opportunity to test the application of NICS2BC to large molecules with complex aromatic behavior. For both molecules, we extracted molecular coordinates and the $NICS(1)_{ZZ}$ values[99] reported by the authors of the original publications and used them to generate predicted bond-currents with NICS2BC. For **Test1**, we compared our results to the reported current density map; for **Test2**, we compared our results to the reported ACID[20] plot. As can be seen in Figure 6, for both cases, not only do our results replicate the current flow calculated by the different current-density methods, but the visualization of the NICS2BC results is substantially clearer to grasp and to interpret via a cursory visual inspection. The main features of the current, as they are obtained directly from the calculation, are plainly seen, and do not require any image manipulation (e.g., image enlargement or overlaying of clarifying arrows). In addition to these advantages, we emphasize that both of these information-rich depictions were obtained without any further quantum chemical calculations on our part.

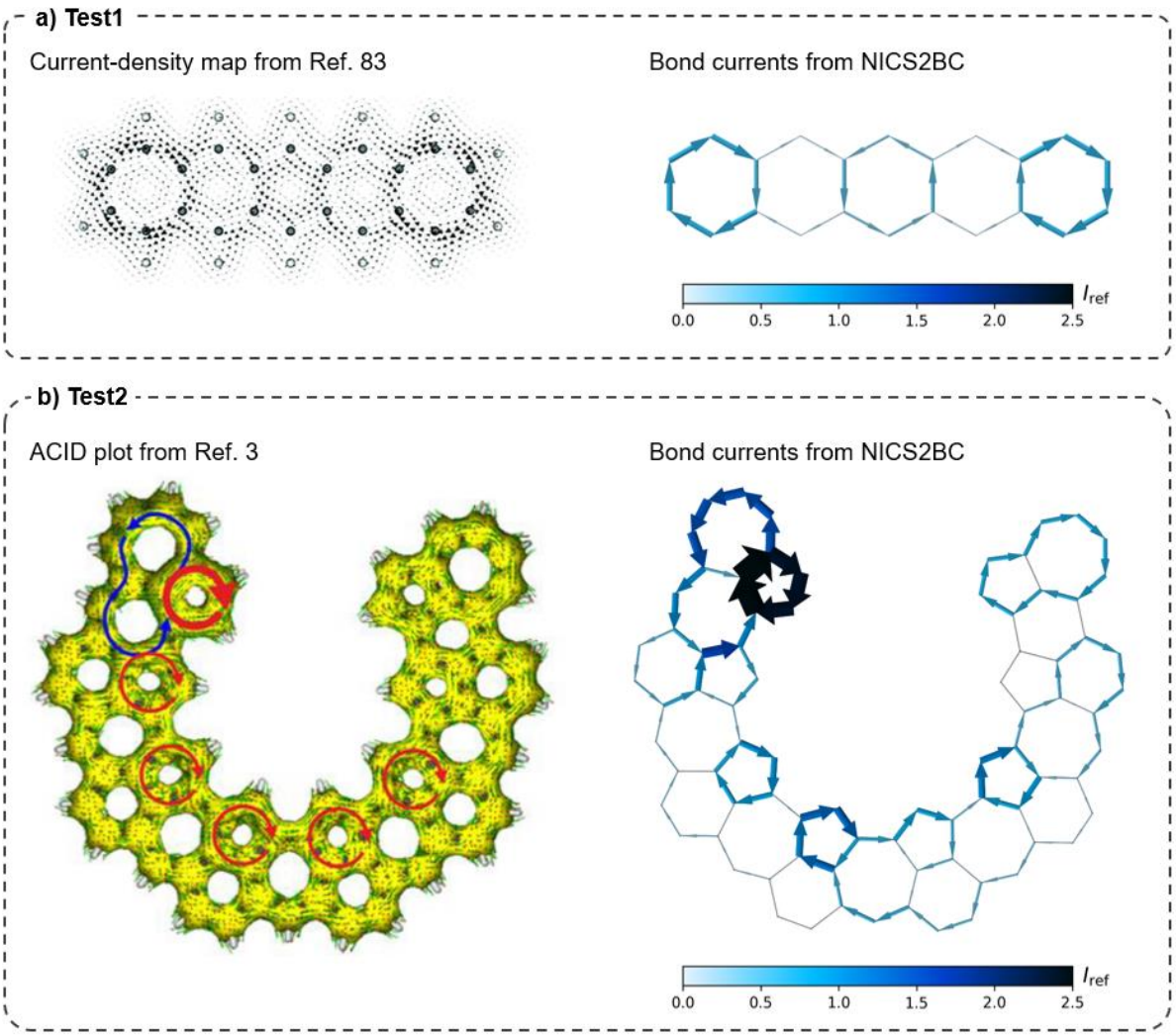

Figure 6. Comparison of different aromaticity visualizations for **Test1** and **Test2**. a) **Test1**: Current-density map (left) and bond-currents generated by NICS2BC (right)**.** B) **Test2:** ACID (left) and bond-currents generated by NICS2BC (right). Left-side images reproduced with permission from References [98] and 3, respectively. NICS2BC current calculated from the reported $NICS(1)_{ZZ}$ values, strength is reported relative to I_{ref} (the ring current of benzene, 11.5 nA T^{-1}).

The results presented here demonstrate that the NICS2BC framework can successfully characterize molecules of various size and aromatic behavior, and that it provides an easy-to-obtain, clear, and accurate depiction of the current flow in both simple and complex molecules.

Limitations of the Method

In the examples described above, we showed the success of NICS2BC in capturing the bond-currents of various types of polycyclic aromatic systems. However, as with any new method, it is natural to seek the boundaries of applicability and to identify inherent limitations.

First and foremost, we emphasize that NICS2BC is dependent on the input NICS values and, therefore, it can only work well in cases that NICS itself works well. If the input NICS values are inaccurate evaluators of a molecule's current density, then the NICS2BC graphs afforded from them will also provide spurious results. For this reason, we recommend users follow the best practices of using NICS, as detailed in Reference 28. In particular, NICS is not appropriate for use with molecules containing transition metals, as noted by Foroutan-Nejad et al.[100,101]

Another limitation stems naturally from our choice of bond-currents as a model for the current density, and is generally true for bond-current representations, regardless of the method of calculation (integration, graph theory, topological methods, or NICS2BC). All bond-current methods are not ideal for cases where there are currents that cannot be mapped to bonds. This can happen, for example, due to cancellation of currents by symmetry (currents of equal strength and opposite directions flowing along the same bond give a net zero current). We show two such examples in the SI: dicationic naphthalene, **CC7**$^{2+}$, and pentalene, **CC16**, in Figures S10 and S12, respectively.

The third limitation is a technical one that affects the applicability of the NICS2BC approach to curved aromatic molecules. In our in-house trials, we have found that the Biot-Savart equation, which is employed in Step 2 (Figure 2) to calculate NICS values from bond-currents, does not provide equally accurate results for non-planar molecules. As a result, the $\tilde{\boldsymbol{\sigma}}$ matrix, and subsequently also the bond-currents, cannot be accurately calculated. We are currently investigating the reason for this inaccuracy and are working towards an alternative approach for generating the $\tilde{\boldsymbol{\sigma}}$ matrix, which will allow NICS2BC to be used safely for curved aromatic molecules.

Conclusions

In this report, we have presented a new method, NICS2BC, which combines the respective advantages of NICS—simple, accessible and relatively inexpensive—and bond-currents—intuitive and quantitative visual representation—to generate clear and informative bond-current graphs of (polycyclic) aromatic molecules. These graphs allow for straightforward characterization of the π-electron currents and avoid many common pitfalls in interpretation of aromatic behavior and allow for evaluation of local aromaticity using NICS. We note that this is the first method to provide an approximation of the π-electron current density using GIAOs.

We have demonstrated the application of NICS2BC on a variety of mono- and polycyclic aromatic compounds comprising various-sized rings, charges, heteroatoms, and aromatic

behaviors. As a further test, we showed that NICS2BC can also successfully deal with open-shell and with large systems (containing 23 rings). Our results show both a quantitative agreement with bond-currents obtained by integration and a qualitative agreement between the interpretation afforded by our graphs and that afforded by current-density maps. The results also demonstrate that NICS2BC is capable of dealing with complex systems, some of which have been incorrectly characterized based solely on NICS.[91,102] This implies that our method recreates information that is lost in the translation of current density to NICS, without having to do any additional quantum chemical computations.

Additionally, we note that the BC-Wizard program in which NICS2BC has been implemented offers additional advantages. Namely, due to the style and clarity of the representation, there is no need for enlarged high-resolution images or additional indications on the image. Furthermore, in addition to the default settings, which are suitable for a wide range of compounds, the program offers customizable settings, enabling the user to easily change the arrow color and size scales to generate NICS2BC maps that best highlight the features of the studied molecules. In the event of weak currents, the scale can be easily modified to enable clear visualization. The program and its accompanying instructions and documentation are freely available on GitLab and are specifically tailored for user-friendliness and customizability.

As a final point, we wish to comment on the weights generated by NICS2BC. As written by Bultinck et al. in 2006, "Ring-specific NICS values would certainly be very powerful quantities for comparison of local aromaticity, but the projection operators or other techniques to do so still remain unknown."[103] Because NICS values are inherently influenced by multiple effects within a polycyclic system, they often disagree with other metrics in the evaluation of local aromaticity.[104,102,91] The weights calculated by NICS2BC, by definition, represent the contribution of each individual ring to the molecular currents. Thus, these values offer an interesting new way to investigate the concept of local aromatic behavior within polycyclic systems. To the best of our knowledge, this is the first demonstration of deconvolution of NICS values to enable ring-specific values. Work is currently underway in our group to make use of these weights for this purpose, and to investigate the relationship between weights and other structural features.

Conflicts of Interest

There are no conflicts to declare.

Acknowledgements

The authors express their deep gratitude to Prof. Peter Chen for his financial and scientific support and for his mentorship, and are also thankful to P. Finkelstein, Dr. A. Tsybizova, and Dr. R. Pollice for fruitful discussions and helpful comments on the manuscript. The ETH Zürich, the Technion, and the Branco Weiss Fellowship are gratefully acknowledged for financial support. R.G.P. is a Branco Weiss Fellow and a Horev Fellow.

Footnote

This manuscript is dedicated with great appreciation to Prof. Riccardo Zanasi on the occasion of his 70th birthday.

References

1 G. I. Warren, J. E. Barker, L. N. Zakharov and M. M. Haley, Enhancing the Antiaromaticity of s-Indacene through Naphthothiophene Fusion, *Org. Lett.*, 2021, **23**, 5012–5017.

2 Q. Fan, L. Yan, M. W. Tripp, O. Krejčí, S. Dimosthenous, S. R. Kachel, M. Chen, A. S. Foster, U. Koert, P. Liljeroth and J. M. Gottfried, Biphenylene network: A nonbenzenoid carbon allotrope, *Science*, 2021, **372**, 852–856.

3 I. C.-Y. Hou, Q. Sun, K. Eimre, M. Di Giovannantonio, J. I. Urgel, P. Ruffieux, A. Narita, R. Fasel and K. Müllen, On-Surface Synthesis of Unsaturated Carbon Nanostructures with Regularly Fused Pentagon–Heptagon Pairs, *J. Am. Chem. Soc.*, 2020, **142**, 10291–10296.

4 M. Irie, *Diarylethene Molecular Photoswitches: Concepts and Functionalities*, John Wiley & Sons, 2021.

5 Y. Qin, G. Li, T. Qi and H. Huang, Aromatic imide/amide-based organic small-molecule emitters for organic light-emitting diodes, *Mater. Chem. Front.*, 2020, **4**, 1554–1568.

6 J. Wang, N. Boens, L. Jiao and E. Hao, Aromatic [b]-fused BODIPY dyes as promising near-infrared dyes, *Org. Biomol. Chem.*, 2020, **18**, 4135–4156.

7 J. E. Anthony, Functionalized acenes and heteroacenes for organic electronics., *Chem. Rev.*, 2006, **106**, 5028–5048.

8 A. Al Ruzaiqi, H. Okamoto, Y. Kubozono, U. Zschieschang, H. Klauk, P. Baran and H. Gleskova, Low-voltage organic thin-film transistors based on [n]phenacenes, *Org. Electron.*, 2019, **73**, 286–291.

9 M. Kim, S. U. Ryu, S. A. Park, K. Choi, T. Kim, D. Chung and T. Park, Donor–Acceptor-Conjugated Polymer for High-Performance Organic Field-Effect Transistors: A Progress Report, *Adv. Funct. Mater.*, 2020, **30**, 1904545.

10 W. Zhao, J. Ding, Y. Zou, C. Di and D. Zhu, Chemical doping of organic semiconductors for thermoelectric applications, *Chem. Soc. Rev.*, 2020, **49**, 7210–7228.

11 M. R. Cavallari, L. M. Pastrana, C. D. F. Sosa, A. M. R. Marquina, J. E. E. Izquierdo, F. J. Fonseca, C. A. de Amorim, L. G. Paterno and I. Kymissis, Organic Thin-Film Transistors as Gas Sensors: A Review, *Materials*, 2021, **14**, 3.

12 P. W. Fowler, P. Hansen, G. Caporossi and A. Soncini, Polyenes with maximum HOMO-LUMO gap, *Chem. Phys. Lett.*, 2001, **342**, 105–112.

13 R. Gershoni-Poranne, A. P. Rahalkar and A. Stanger, The predictive power of aromaticity: quantitative correlation between aromaticity and ionization potentials and HOMO–LUMO gaps in oligomers of benzene, pyrrole, furan, and thiophene, *Phys. Chem. Chem. Phys.*, 2018, **20**, 14808–14817.

14 S. Ito and M. Nakano, Theoretical Molecular Design of Heteroacenes for Singlet Fission: Tuning the Diradical Character by Modifying π-Conjugation Length and Aromaticity, *J. Phys. Chem. C*, 2015, **119**, 148–157.

15 D. Chen, T. Shen, K. An and J. Zhu, Adaptive aromaticity in S 0 and T 1 states of pentalene incorporating 16 valence electron osmium, *Commun. Chem.*, 2018, **1**, 1–7.

16 O. El Bakouri, J. R. Smith and H. Ottosson, Strategies for Design of Potential Singlet Fission Chromophores Utilizing a Combination of Ground-State and Excited-State Aromaticity Rules, *J. Am. Chem. Soc.*, 2020, **142**, 5602–5617.

17 K. B. Vu, T. Le Phuc Nhi, V. V. Vu and S. Tung Ngo, How do magnetic, structural, and electronic criteria of aromaticity relate to HOMO – LUMO gap? An evaluation for graphene quantum dot and its derivatives, *Chem. Phys.*, 2020, **539**, 110951.

18 G. Markert, E. Paenurk and R. Gershoni-Poranne, Prediction of Spin Density, Baird-Antiaromaticity, and Singlet–Triplet Energy Gap in Triplet-State Polybenzenoid Systems from Simple Structural Motifs, *Chem. – Eur. J.*, 2021, **27**, 1–14.

19 I. Fernandez, Ed., *Aromaticity: Modern Computational Methods and Applications*, Elsevier, 2021.
20 D. Geuenich, K. Hess, F. Köhler and R. Herges, Anisotropy of the Induced Current Density (ACID), a General Method To Quantify and Visualize Electronic Delocalization, *Chem. Rev.*, 2005, **105**, 3758–3772.
21 H. Fliegl, S. Taubert, O. Lehtonen and D. Sundholm, The gauge including magnetically induced current method, *Phys. Chem. Chem. Phys.*, 2011, **13**, 20500–20518.
22 D. Sundholm, H. Fliegl and R. J. F. Berger, Calculations of magnetically induced current densities: theory and applications, *WIREs Comput. Mol. Sci.*, 2016, **6**, 639–678.
23 M. Hegarty, The Cognitive Science of Visual-Spatial Displays: Implications for Design, *Top. Cogn. Sci.*, 2011, **3**, 446–474.
24 R. Hoffmann and P. Laszlo, Representation in Chemistry, *Angew. Chem. Int. Ed.*, 1991, **30**, 1–16.
25 M. Valle, Visualization: A cognition amplifier, *Int. J. Quantum Chem.*, 2013, **113**, 2040–2052.
26 S. Akaygun and L. L. Jones, Words or Pictures: A comparison of written and pictorial explanations of physical and chemical equilibria, *Int. J. Sci. Educ.*, 2014, **36**, 783–807.
27 R. Pollice and P. Chen, A Universal Quantitative Descriptor of the Dispersion Interaction Potential, *Angew. Chem. Int. Ed.*, 2019, **58**, 9758–9769.
28 C. E. Colwell, T. W. Price, T. Stauch and R. Jasti, Strain visualization for strained macrocycles, *Chem. Sci.*, 2020, **11**, 3923–3930.
29 B. J. Lampkin, P. B. Karadakov and B. VanVeller, Detailed Visualization of Aromaticity Using Isotropic Magnetic Shielding, *Angew. Chem. Int. Ed.*, 2020, **59**, 19275–19281.
30 Z. Chen, C. S. Wannere, C. Corminboeuf, R. Puchta and P. von R. Schleyer, Nucleus-Independent Chemical Shifts (NICS) as an Aromaticity Criterion, *Chem. Rev.*, 2005, **105**, 3842–3888.
31 R. Gershoni-Poranne and A. Stanger, in *Aromaticity: Modern Computational Methods and Applications*, ed. I. Fernandez, Elsevier, 2021, pp. 99–154.
32 J. Kruszewski and T. M. Krygowski, Definition of aromaticity based on the harmonic oscillator model, *Tetrahedron Lett.*, 1972, **36**, 3839–42.
33 T. M. Krygowski and M. K. Cyranski, Structural Aspects of Aromaticity, *Chem. Rev.*, 2001, **101**, 1385–1419.
34 E. Matito, M. Duran and M. Solà, The aromatic fluctuation index (FLU): A new aromaticity index based on electron delocalization, *J. Chem. Phys.*, 2005, **122**, 014109.
35 M. Giambiagi, M. Segre de Giambiagi, C. D. dos Santos Silva and A. Paiva de Figueiredo, Multicenter bond indices as a measure of aromaticity, *Phys. Chem. Chem. Phys.*, 2000, **2**, 3381–3392.
36 T. Lu and F. Chen, Multiwfn: A multifunctional wavefunction analyzer, *J. Comput. Chem.*, 2012, **33**, 580–592.
37 G. Monaco, F. F. Summa and R. Zanasi, Program Package for the Calculation of Origin-Independent Electron Current Density and Derived Magnetic Properties in Molecular Systems, *J. Chem. Inf. Model.*, , DOI:10.1021/acs.jcim.0c01136.
38 J. Aihara, Aromaticity and diatropicity, *Pure Appl Chem*, 1982, **54**, 1115–28.
39 J. Aihara, Magnetotropism of biphenylene and related hydrocarbons. A circuit current analysis, *J. Am. Chem. Soc.*, 1985, **107**, 298–302.
40 J. A. N. F. Gomes and R. B. Mallion, Aromaticity and Ring Currents, *Chem. Rev.*, 2001, **101**, 1349–1383.
41 R. Carion, B. Champagne, G. Monaco, R. Zanasi, S. Pelloni and P. Lazzeretti, Ring Current Model and Anisotropic Magnetic Response of Cyclopropane, *J. Chem. Theory Comput.*, 2010, **6**, 2002–2018.

42 T. K. Dickens and R. B. Mallion, π-Electron ring-currents and bond-currents in [10,5]-Coronene and related structures conforming to the 'Annulene-Within-an-Annulene' model, *Phys. Chem. Chem. Phys.*, 2013, **15**, 8245–8253.
43 T. K. Dickens and R. B. Mallion, Topological Hückel–London–Pople–McWeeny Ring Currents and Bond Currents in altan-Corannulene and altan-Coronene, *J. Phys. Chem. A*, 2014, **118**, 933–939.
44 T. K. Dickens and R. B. Mallion, Topological Ring Currents and Bond Currents in Some Neutral and Anionic Altans and Iterated Altans of Corannulene and Coronene, *J. Phys. Chem. A*, 2018, **122**, 7666–7678.
45 M. Antić, S. Đorđević, B. Furtula and S. Radenković, Magnetically Induced Current Density in Non-Planar Fully Benzenoid Hydrocarbons, *J. Phys. Chem. A*, , DOI:10.1021/acs.jpca.9b10352.
46 T. K. Dickens and R. B. Mallion, Topological Ring-Currents and Bond-Currents in Hexaanionic Altans and Iterated Altans of Corannulene and Coronene, *J. Phys. Chem. A*, 2020, **124**, 7973–7990.
47 M. O. Hamzah, M. S. Hadi, S. H. Saleh, I. M. M. Hassan, S. F. Nareen and I. A. Hussen, A comparative study of bond currents of some benzenoids using Hückel-London, Spanish and Polish models, 2020, 020009.
48 R. Pino-Rios, A. Vásquez-Espinal, O. Yañez and W. Tiznado, Searching for double σ- and π-aromaticity in borazine derivatives, *RSC Adv.*, 2020, **10**, 29705–29711.
49 S. Radenković and S. Đorđević, Relating nucleus independent chemical shifts with integrated current density strengths, *Phys. Chem. Chem. Phys.*, 2021, **23**, 11240–11250.
50 M. Orozco-Ic and G. Merino, The Magnetic Response of Starphenes, *Chemistry*, 2021, **3**, 1381–1391.
51 M. Orozco-Ic, M. Dimitrova, J. Barroso, D. Sundholm and G. Merino, Magnetically Induced Ring-Current Strengths of Planar and Nonplanar Molecules: New Insights from the Pseudo-π Model, *J. Phys. Chem. A*, 2021, **125**, 5753–5764.
52 T. J. P. Irons, L. Spence, G. David, B. T. Speake, T. Helgaker and A. M. Teale, Analyzing Magnetically Induced Currents in Molecular Systems Using Current-Density-Functional Theory, *J. Phys. Chem. A*, 2020, **124**, 1321–1333.
53 R. J. F. Berger, M. Dimitrova, R. T. Nasibullin, R. R. Valiev and D. Sundholm, Integration of global ring currents using the Ampère–Maxwell law, *Phys. Chem. Chem. Phys.*, 2022, **24**, 624–628.
54 J. Aihara, Graph theory of ring-current diamagnetism, *Bull Chem Soc Jpn*, 2017, **91**, 274–303.
55 T. K. Dickens, J. A. N. F. Gomes and R. B. Mallion, Some Comments on Topological Approaches to the π-Electron Currents in Conjugated Systems, *J. Chem. Theory Comput.*, 2011, **7**, 3661–3674.
56 T. K. Dickens and R. B. Mallion, Topological Ring-Currents in Conjugated Systems, *MATCH Commun. Math. Comput. Chem.*, 2016, **76**, 297–356.
57 P. v R. Schleyer, C. Maerker, A. Dransfeld, H. Jiao and N. J. R. van Eikema Hommes, Nucleus-independent chemical shifts: a simple and efficient aromaticity probe, *J. Am. Chem. Soc.*, 1996, **118**, 6317–6318.
58 A. Stanger, NICS – Past and Present, *Eur. J. Org. Chem.*, 2020, **21**, 3120–3127.
59 L. Pauling, The Diamagnetic Anisotropy of Aromatic Molecules, *J. Chem. Phys.*, 1936, **4**, 673–677.
60 K. Y. Lonsdale and W. H. Bragg, Magnetic anisotropy and electronic structure of aromatic molecules, *Proc. R. Soc. Lond. Ser. - Math. Phys. Sci.*, 1937, **159**, 149–161.
61 F. London, Théorie quantique des courants interatomiques dans les combinaisons aromatiques, *J Phys Radium*, 1937, **8**, 397–409.

62 J. A. Pople, Molecular orbital theory of aromatic ring currents, *Mol. Phys.*, 1958, **1**, 175–180.
63 R. McWeeny, Ring currents and proton magnetic resonance in aromatic molecules, *Mol. Phys.*, 1958, **1**, 311–321.
64 R. Islas, G. Martínez-Guajardo, J. O. C. Jiménez-Halla, M. Solà and G. Merino, Not All That Has a Negative NICS Is Aromatic: The Case of the H-Bonded Cyclic Trimer of HF, *J. Chem. Theory Comput.*, 2010, **6**, 1131–1135.
65 M. Solà, Why Aromaticity Is a Suspicious Concept? Why?, *Front. Chem.*, 2017, **5**, 22.
66 R. Gershoni-Poranne and A. Stanger, The NICS-XY-Scan: Identification of Local and Global Ring Currents in Multi- Ring Systems, *Chem. – Eur. J.*, 2014, **20**, 5673–5688.
67 S. Klod and E. Kleinpeter, Ab initio calculation of the anisotropy effect of multiple bonds and the ring current effect of arenes—application in conformational and configurational analysis, *J. Chem. Soc. Perkin Trans. 2*, 2001, 1893–1898.
68 D. Inostroza, V. García, O. Yañez, J. J. Torres-Vega, A. Vásquez-Espinal, R. Pino-Rios, R. Báez-Grez and W. Tiznado, On the NICS limitations to predict local and global current pathways in polycyclic systems, *New J. Chem.*, 2021, **45**, 8345–8351.
69 M. J. Frisch, G. W. Trucks, H. B. Schlegel, G. E. Scuseria, M. A. Robb, J. R. Cheeseman, G. Scalmani, V. Barone, B. Mennucci, G. A. Petersson, and et al., Gaussian 09, Revision D.01, *Gaussian Inc Wallingford CT*.
70 A. D. Becke, Density-functional thermochemistry. III. The role of exact exchange, *J. Chem. Phys.*, 1993, **98**, 5648–5652.
71 C. Lee, W. Yang and R. G. Parr, Development of the Colle-Salvetti correlation-energy formula into a functional of the electron density, *Phys. Rev. B*, 1988, **37**, 785.
72 S. H. Vosko, L. Wilk and M. Nusair, Accurate spin-dependent electron liquid correlation energies for local spin density calculations: a critical analysis, *Can. J. Phys.*, 1980, **58**, 1200–1211.
73 R. H. Hertwig and W. Koch, On the parameterization of the local correlation functional. What is Becke-3-LYP?, *Chem. Phys. Lett.*, 1997, **268**, 345–351.
74 F. Weigend and R. Ahlrichs, Balanced basis sets of split valence, triple zeta valence and quadruple zeta valence quality for H to Rn: Design and assessment of accuracy, *Phys. Chem. Chem. Phys.*, 2005, **7**, 3297.
75 S. Grimme, J. Antony, S. Ehrlich and H. Krieg, A consistent and accurate ab initio parametrization of density functional dispersion correction (DFT-D) for the 94 elements H-Pu, *J. Chem. Phys.*, 2010, **132**, 154104.
76 J. A. Bohmann, F. Weinhold and T. C. Farrar, Natural chemical shielding analysis of nuclear magnetic resonance shielding tensors from gauge-including atomic orbital calculations, *J. Chem. Phys.*, 1997, **107**, 1173–1184.
77 E. D. Glendening, C. R. Landis and F. Weinhold, Natural bond orbital methods, *WIREs Comput. Mol. Sci.*, 2012, **2**, 1–42.
78 E. D. Glendening, C. R. Landis and F. Weinhold, NBO 6.0: Natural bond orbital analysis program, *J. Comput. Chem.*, 2013, **34**, 1429–1437.
79 T. A. Keith and R. F. W. Bader, Calculation of magnetic response properties using a continuous set of gauge transformations, *Chem. Phys. Lett.*, 1993, **210**, 223–231.
80 E. Paenurk, S. Feusi and R. Gershoni-Poranne, Predicting bond-currents in polybenzenoid hydrocarbons with an additivity scheme, *J. Chem. Phys.*, 2021, **154**, 024110.
81 S. Van Damme, G. Acke, R. W. A. Havenith and P. Bultinck, Can the current density map topology be extracted from the nucleus independent chemical shifts?, *Phys. Chem. Chem. Phys.*, 2016, **18**, 11746–11755.
82 *Classical Electrodynamics*, John Wiley & Sons, Inc., 1998.

83 A. Zamora, An Algorithm for Finding the Smallest Set of Smallest Rings, *J. Chem. Inf. Model.*, 1976, **16**, 40–43.
84 J. Jusélius, D. Sundholm and J. Gauss, Calculation of current densities using gauge-including atomic orbitals, *J. Chem. Phys.*, 2004, **121**, 3952–3963.
85 E. Steiner and P. W. Fowler, Patterns of Ring Currents in Conjugated Molecules: A Few-Electron Model Based on Orbital Contributions, *J Phys Chem A*, 2001, **105**, 9553–9562.
86 H. Fallah-Bagher-Shaidaei, C. S. Wannere, C. Corminboeuf, R. Puchta and P. v R. Schleyer, Which NICS Aromaticity Index for Planar π Rings Is Best?, *Org. Lett.*, 2006, **8**, 863–866.
87 R. Báez-Grez, L. Ruiz, R. Pino-Rios and W. Tiznado, Which NICS method is most consistent with ring current analysis? Assessment in simple monocycles, *RSC Adv.*, 2018, **8**, 13446–13453.
88 A. Stanger, G. Monaco and R. Zanasi, NICS-XY-Scan Predictions of Local, Semi-Global, and Global Ring Currents in Annulated Pentalene and s-Indacene Cores Compared to First-Principles Current Density Maps, *ChemPhysChem*, 2020, **21**, 65–82.
89 M. Randic, Aromaticity of Polycyclic Conjugated Hydrocarbons, *Chem. Rev.*, 2003, **103**, 3449–3605.
90 S. Fias, P. W. Fowler, J. L. Delgado, U. Hahn and P. Bultinck, Correlation of Delocalization Indices and Current-Density Maps in Polycyclic Aromatic Hydrocarbons, *Chem. – Eur. J.*, 2008, **14**, 3093–3099.
91 J. Poater, M. Sola, R. G. Viglione and R. Zanasi, Local Aromaticity of the Six-Membered Rings in Pyracylene. A Difficult Case for the NICS Indicator of Aromaticity, *J. Org. Chem.*, 2004, **69**, 7537–7542.
92 E. Steiner and P. W. Fowler, Ring Currents in the Porphyrins: A Four-Orbital Model, *ChemPhysChem*, 2002, **3**, 114–116.
93 W. E. Barth and R. G. Lawton, Dibenzo[ghi,mno]fluoranthene, *J. Am. Chem. Soc.*, 1966, **88**, 380–381.
94 M. Baumgarten, L. Gherghel, M. Wagner, A. Weitz, M. Rabinovitz, P.-C. Cheng and L. T. Scott, Corannulene Reduction: Spectroscopic Detection of All Anionic Oxidation States, *J. Am. Chem. Soc.*, 1995, **117**, 6254–6257.
95 E. Steiner, P. W. Fowler and L. W. Jenneskens, Counter-Rotating Ring Currents in Coronene and Corannulene, *Angew. Chem. Int. Ed.*, 2001, **40**, 362–366.
96 J. Aihara, Circuit Resonance Energy: A Key Quantity That Links Energetic and Magnetic Criteria of Aromaticity, *J. Am. Chem. Soc.*, 2006, **128**, 2873–2879.
97 A. Kumar, M. Duran and M. Solà, Is coronene better described by Clar's aromatic π-sextet model or by the AdNDP representation?, *J. Comput. Chem.*, 2017, **38**, 1606–1611.
98 R. Pino-Rios, R. Báez-Grez and M. Solà, Acenes and phenacenes in their lowest-lying triplet states. Does kinked remain more stable than straight?, *Phys. Chem. Chem. Phys.*, , DOI:10.1039/D1CP01441B.
99 According to our quantitative analysis, $NICS(1)_{ZZ}$ provides bond currents that are comparably accurate to those based on $NICS(1.25)_{ZZ}$ (see Section S4.2 in the SI for further details), therefore there was no reason not to use the values reported by the author. To generate comparable NICS2BC maps, we normalized these using the I_{ref} of benzene calculated at the same level of theory and height.
100 C. Foroutan-Nejad, Is NICS a reliable aromaticity index for transition metal clusters?, *Theor Chem Acc*, 2015, **134**, 8.
101 C. Foroutan-Nejad, J. Vícha and A. Ghosh, Relativity or aromaticity? A first-principles perspective of chemical shifts in osmabenzene and osmapentalene derivatives, *Phys. Chem. Chem. Phys.*, , DOI:10.1039/D0CP01481H.
102 P. Bultinck, Critical analysis of the local aromaticity concept in polyaromatic hydrocarbons, *Faraday Discuss.*, 2007, **135**, 347–365.

103 P. Bultinck, S. Fias and R. Ponec, Local aromaticity in polycyclic aromatic hydrocarbons: electron delocalization versus magnetic indices, *Chem - Eur J*, 2006, **12**, 8813–8818.
104 G. Portella, J. Poater, J. M. Bofill, P. Alemany and M. Sola, Local Aromaticity of [n]acenes, [n]phenacenes, and [n]helicenes (n = 1-9), *J. Org. Chem.*, 2005, **70**, 2509–2521.